Solvent-free, molecular-level modeling of self-assembling amphiphiles in water

Somajit Dey* and Jayashree Saha†
Department of Physics, University of Calcutta, 92, A.P.C. Road, Kolkata-700009, India
(Received 25 October 2016; revised manuscript received 29 January 2017; published 28 February 2017)

Aggregation mesophases of self-assembling amphiphiles in water are highly important in the context of biology (biomembranes), therapy (liposomes), industry (polymer surfactants), and condensed-matter physics (lyotropic liquid crystals). Besides helping to increase fundamental understanding of collective molecular behavior, simulations of these lyotropic phases are pivotal to technological and medical developments such as smart drug carriers for gene therapy. Implicit-solvent, coarse-grained, low resolution modeling with a simple pair potential is the key to realizing the larger length and time scales associated with such mesoscopic phenomena during a computer simulation. Modeling amphiphiles by directed, soft, ellipsoidal cores interacting via a computationally simple yet tunable anisotropic pair potential, we have come to such a single-site model amphiphile that can rapidly self-assemble to give diverse lyotropic phases (such as fluid bilayers, micelles, etc.) without requiring the explicit incorporation of solvent particles. The model directly represents a tunable packing parameter that manifests in the spontaneous curvature of the amphiphile aggregates. Besides the all-important hydrophobic interaction, the hydration force is also treated implicitly. Thanks to the efficient solvent-free molecular-level coarse graining, this model is suitable for generic mesoscale studies of phenomena such as self-assembly, amphiphile mixing, domain formation, fusion, elasticity, etc., in amphiphile aggregates.

DOI: 10.1103/PhysRevE.95.023315

I. INTRODUCTION

Amphiphiles (such as lipids and surfactants) are macromolecules consisting of a hydrophilic (water-loving) head linked to one or more hydrophobic (water-hating) chains (tails). Phenomena associated with water solution of amphiphiles span many scales in length and time. At extreme dilution the amphiphiles get adsorbed at the water surface or stay dispersed as monomers. Above a certain temperature (Krafft point) and a certain concentration (critical micelle concentration) single-chain surfactants self-assemble into micelles [1–5]. Spherical, elliptical and cylindrical micelles have been observed [6,7]. With increasing concentration (and/or varying temperature), the amphiphiles are known to generate a variety of ordered aggregation phases such as tubular middle phase, neat phase from lamellar bilayers, cubic phase, sponge phase, multiply connected bilayers, etc. [6,8,9]. The importance of these lyotropic liquid crystals [6] cannot be overestimated in physical, biological, therapeutic, and industrial contexts. Analysis of the relevant processes are, however, very challenging due to the complexity of the interactions and the fact that many scales are involved simultaneously. Computer simulation, therefore, holds a very special place in the study of amphiphile aggregates. Since atomistic computer simulations employ the most detailed and chemically specific models, they are unable to probe, within viable processor time, the largest length and time scales associated with events such as self-assembly into aggregates, amphiphile mixing, fusion of aggregates, etc. [10]. Moreover, complete atomistic detail may actually obscure the fundamental mechanisms underlying these processes providing no significant insight into them. We, therefore, need coarse-grained (CG) models of lower resolutions with inherent time and length scales not too small compared to the scales to be probed. Coarsening of models by elimination of some of the degrees of freedom smooths the phase-space energy surface and speeds up dynamics by allowing larger time steps [10]. It also reduces the number of site-site interactions for a given number of macromolecules implying a larger length scale and lesser expensive force computations at each step. However, the small size of CG water molecules compared to the amphiphiles, combined with their multitude (∼10 CG water particles per amphiphile), still limits the scales of a simulation as most processor time is spent computing the solvent interactions and movements. Yet most CG water models act merely as mediators of an effective hydrophobic bonding [11,12] so that stable amphiphile aggregates can be achieved. Implicit-solvent (IS) or solvent-free amphiphile models do away with this CG water by mimicking the solvent-mediated interactions with some specialized interparticle force field instead [10]. An ISCG model thereby speeds up the computation manifold as it concentrates only on the amphiphiles and, hence, offers a means to look into the largest time and length scales associated with amphiphile aggregates. Almost all ISCG models that show successful unassisted self-assembly constitute the amphiphiles from a number of beads of different species (hydrophilic, hydrophobic, linker, etc.) linked by flexible interbead bonds [13–16]. Although the beads interact among themselves by simple force laws, the models are invariably multisite and, hence, computationally expensive compared to some simple molecular-level single-site model. Such a molecular-level model, therefore, promises the largest scales for qualitative simulations [17].

Anisotropic single-site coarse graining, with several parameters, is often used in computational physics to replace a linear array of beads efficiently [18,19]. Far from leading to an impoverishment of the model, this might turn out to give rise to some very interesting physical behavior [20]. Self-assembly into stable aggregates (including fluid bilayers) is, however, a great challenge for single-site IS models with

*dey.somajit@gmail.com
†jsphy@caluniv.ac.in

simple pair potentials [21]. To the best of our knowledge, only two attempts in this direction [22,23] have been reported so far. Although Ref. [22] models a tunable phase curvature (packing parameter [24,25]) successfully, it does so at the expense of self-assembly. It also suffers drawbacks in that unphysical monolayers (sometimes with domains of alternating head-tail orientations) are allowed within bulk solvent for some values of the parameters and hydration force [26] is not accounted for. The relatively simpler model by Noguchi [23], however, never compromises self-assembly.

The present paper gives a single-site IS model that is unique in its direct representation of a tunable packing parameter without compromising self-assembly. Hydration force is also modeled and monolayers within bulk water are energetically unfavorable. Diverse stable phases of non-negative curvature (e.g., fluid lamellar bilayers, spherical micelles, etc.) are obtained in computer simulations proving the model appropriate for qualitative mesoscale studies of amphiphile aggregates in water.

II. MODEL

Our model amphiphile consists of a soft-core, directed, prolate spheroid of tunable length with a tunable anisotropic force field. Here, actually, we make use of the approximate spheroid geometry that appears in the popular Gay-Berne (GB) force field [18]. Taking two identical uniaxial spheroids i and j with centers at $\mathbf{r}_i$ and $\mathbf{r}_j$ and directed major (or minor) axis along unit vectors $\hat{\mathbf{u}}_i$ and $\hat{\mathbf{u}}_j$, the GB ellipsoidal contact distance is given by

$$\sigma_{\rm GB}(\hat{\mathbf{r}},\hat{\mathbf{u}}_i,\hat{\mathbf{u}}_j) = \sigma_0\left\{1-\frac{1}{2}\chi\left[\frac{(\hat{\mathbf{r}}\cdot\hat{\mathbf{u}}_i+\hat{\mathbf{r}}\cdot\hat{\mathbf{u}}_j)^2}{1+\chi(\hat{\mathbf{u}}_i\cdot\hat{\mathbf{u}}_j)}+\frac{(\hat{\mathbf{r}}\cdot\hat{\mathbf{u}}_i-\hat{\mathbf{r}}\cdot\hat{\mathbf{u}}_j)^2}{1-\chi(\hat{\mathbf{u}}_i\cdot\hat{\mathbf{u}}_j)}\right]\right\}^{-1/2}, \quad (1)$$

where $\hat{\mathbf{r}} = (\mathbf{r}_i - \mathbf{r}_j)/r$, r being the center-center distance. Above, the anisotropy parameter χ is given by $[(\sigma_e/\sigma_s)^2-1]/[(\sigma_e/\sigma_s)^2+1]$ where the parameter $\sigma_e(\sigma_s)$ means the end-end (side-side) contact distance. $\sigma_{\rm GB}$, scaled by $\sigma_0\,(=\sigma_s)$, determines the steric profile of the GB ellipsoid. The well depth of the GB potential contains an energy ellipsoidal term

$$\varepsilon_{\rm GB}(\hat{\mathbf{r}},\hat{\mathbf{u}}_i,\hat{\mathbf{u}}_j) = 1-\frac{1}{2}\chi'\left[\frac{(\hat{\mathbf{r}}\cdot\hat{\mathbf{u}}_i+\hat{\mathbf{r}}\cdot\hat{\mathbf{u}}_j)^2}{1+\chi'(\hat{\mathbf{u}}_i\cdot\hat{\mathbf{u}}_j)}+\frac{(\hat{\mathbf{r}}\cdot\hat{\mathbf{u}}_i-\hat{\mathbf{r}}\cdot\hat{\mathbf{u}}_j)^2}{1-\chi'(\hat{\mathbf{u}}_i\cdot\hat{\mathbf{u}}_j)}\right]. \quad (2)$$

χ' is related to the anisotropy in well depth: for the end-end configuration, $\varepsilon_{\rm GB}$ becomes $\varepsilon_e = (1-\chi')/(1+\chi')$.

Figure 1 depicts the directed spheroid that we envisage. As indicated, $\hat{\mathbf{u}}$, i.e., the unit vector along the directed major axis of our model prolate spheroid, is taken to concur with the built-in directionality of the inversion asymmetric amphiphile: tail to headgroup. Taking $R = (r-\sigma_{\rm GB}+\sigma_0)/\sigma_0$, our model potential, scaled by energy ε_0, reads

$$V(r,\hat{\mathbf{r}},\hat{\mathbf{u}}_i,\hat{\mathbf{u}}_j) = 4\varepsilon_0\left(\frac{1}{R^{12}}-\frac{1}{R^6}\right)+\varepsilon_0-\varepsilon_{\rm wd}(\hat{\mathbf{r}},\hat{\mathbf{u}}_i,\hat{\mathbf{u}}_j), \quad \text{if } r < r_l$$

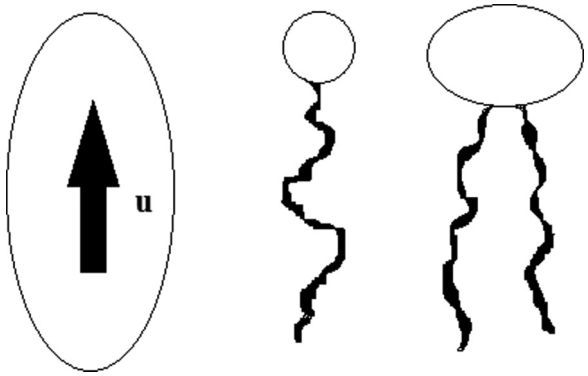

FIG. 1. Our implicit-solvent model amphiphile: a directed spheroid. Directionality (arrow) indicated by single- and double-chain amphiphiles. The spheroids interact through parametrized potentials. The spheroids pack like cones (with angles depending on the choices of parameters), mimicking hydrated amphiphiles with equilibrium headgroup area larger than the tail cross section [see Fig. 5(b)].

$$= s(r)\varepsilon_{\rm wd}(\hat{\mathbf{r}},\hat{\mathbf{u}}_i,\hat{\mathbf{u}}_j), \quad \text{if } r_l \leqslant r < r_u$$
$$= 0, \quad \text{otherwise.} \quad (3)$$

Above, $r_l = (2^{1/6}-1)\sigma_0+\sigma_{\rm GB}$ and $r_u = r_l + range$, where $range$ signifies the tunable range of interaction. $s(r)$ is a cubic switching function [27]:

$$s(r) = (r_u - r)^2(3r_l - 2r - r_u)/range^3. \quad (4)$$

The anisotropic well-depth function $\varepsilon_{\rm wd}(\hat{\mathbf{r}},\hat{\mathbf{u}}_i,\hat{\mathbf{u}}_j)$ is given as

$$\varepsilon_{\rm wd} = \varepsilon_0[\nu_1(\hat{\mathbf{u}}_i\cdot\hat{\mathbf{u}}_j)+\nu_2(\hat{\mathbf{u}}_i\cdot\hat{\mathbf{r}}-\hat{\mathbf{u}}_j\cdot\hat{\mathbf{r}}) - \nu_3(\hat{\mathbf{u}}_i\cdot\hat{\mathbf{r}})(\hat{\mathbf{u}}_j\cdot\hat{\mathbf{r}})+1]^{\nu_0}\varepsilon_{\rm GB}; \quad (5)$$

ν_0, ν_1, ν_2, ν_3 are four parameters to be input externally along with the parameter ε_e associated with $\varepsilon_{\rm GB}(\hat{\mathbf{r}},\hat{\mathbf{u}}_i,\hat{\mathbf{u}}_j)$ [Eq. (2)].

For any set of $(\hat{\mathbf{r}},\hat{\mathbf{u}}_i,\hat{\mathbf{u}}_j)$ the generic r dependence of our model potential is shown in Fig. 2. The attractive tail of $V(r)$ is broader compared to the Lennard-Jones-like r^{-6} form. Empirically it is known that this slower decay is a

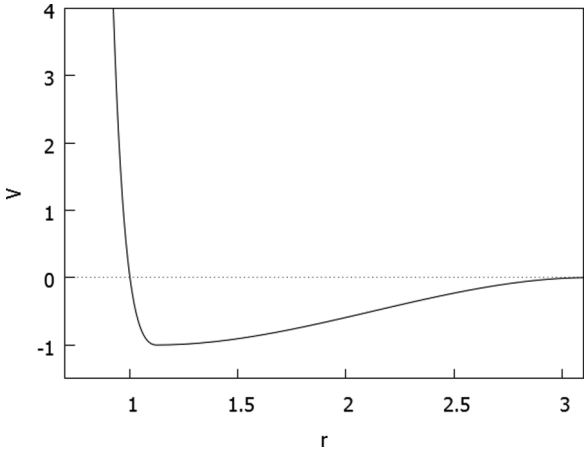

FIG. 2. $V(r)$ [Eq. (3)] for some choice of $(\hat{\mathbf{r}},\hat{\mathbf{u}}_i,\hat{\mathbf{u}}_j)$ such that $\sigma_{\rm GB} = \sigma_0 = 1$ and $\varepsilon_{\rm wd} = \varepsilon_0 = 1$; $range = 2$.

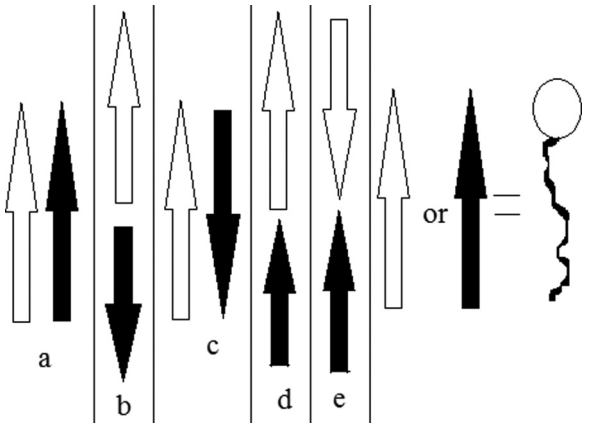

FIG. 3. Relative orientations of amphiphiles in order of decreasing preference from a to e. Directed arrow significance also shown with a single-chain surfactant cartoon. Black and white amphiphiles (arrows) can be of the same or different species.

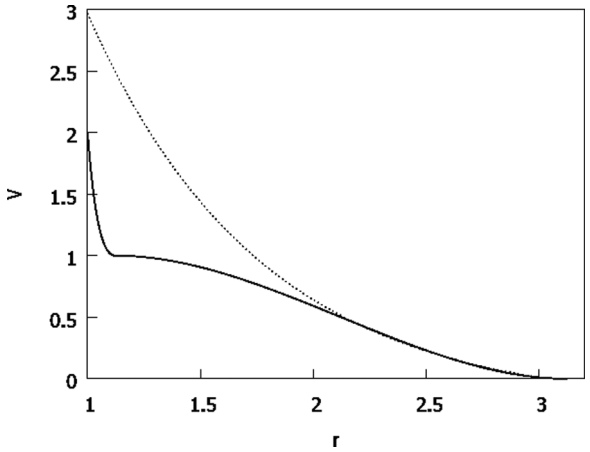

FIG. 4. $V(r)$ [Eq. (3)] for some choice of $(\hat{\mathbf{r}},\hat{\mathbf{u}}_i,\hat{\mathbf{u}}_j)$ such that $\sigma_{GB} = \sigma_0 = 1$ and $\varepsilon_{wd} = \varepsilon_0 = -1$; $range = 2$. The dotted line depicts an exponential fitted to the tail part.

necessity for ISCG models based on pair potentials since stable fluid bilayers are not obtained otherwise [21,28]. The *range* parameter offers a tunable thermal stability of the amphiphile aggregates as in the other models in the literature with a tunable range [21].

In amphiphile aggregates, the hydrophobic bulk is sequestered from the polar solvent by oil-water interfaces. Free-energy gain in transfer of hydrophobic chains from water to oily bulk is the main drive behind surfactant self-assembly [29–32]. Formation of the water-hydrocarbon interface and headgroup repulsion, however, act against it [32,33]. Loss of entropy due to orientational confinement in aggregates also acts as a limiting cause [32]. We modeled the net effect with directed amphiphiles interacting through short range forces favoring certain relative orientations to others. Figure 3 shows five of these orientations in order of decreasing preference from left to right with arrows directed towards the headgroup from the tail of the amphiphile. Phenomenology suggests that the side-side parallel configuration of two surfactants a should be more favorable than the corresponding antiparallel configuration c, as flipping of amphiphiles is a relatively rare phenomenon within amphiphile aggregates. End-end antiparallel configuration with hydrophilic heads away from each other, b, is similarly favorable compared to c. However, hydrophobic interaction and lipophilic (oil-loving) cohesion favors a over b. Hydration pressure, repelling hydrated head groups in the vicinity of each other, makes the end-end headgroup facing configuration e unfavorable compared to c. Hydrophobic and lipophilic interactions also suggest that the end-end parallel configuration d should be favorable compared to e but unfavorable compared to c.

Orientational preferences, as in Fig. 3, are achieved in our model via differences in well depths for different orientations. For example, interamphiphile repulsions in configurations d and e in Fig. 3 are modeled with negative well depths (Fig. 4). A familiar interaction where relative orientations of two directed vectors are energetically distinguished is the dipole-dipole interaction. The first and third terms within square brackets in Eq. (5) are actually inspired by similar terms in the dipole-dipole interaction. It may also be noted that the repulsive tail in Fig. 4 can be approximated as an exponential decay reminiscent of the exponential distance dependence of the hydration forces [26].

Well depth for the cross (X) configuration of the two spheroids is ε_0 from Eq. (5). If the well depth for the a and c configurations are given, respectively, as wd_a and wd_c, then [Eq. (5)]

$$wd_a = \varepsilon_0(\nu_1 + 1)^{\nu_0}, \tag{6}$$

$$wd_c = \varepsilon_0(1 - \nu_1)^{\nu_0}. \tag{7}$$

Solving these gives ν_0 and ν_1. It is, however, necessary that ν_0 be odd as otherwise the negative well depths required to produce repulsions will never be generated. Knowledge of well depths corresponding to the remaining three configurations in Fig. 3, similarly, gives ν_2, ν_3, and ε_e. In other words, the five parameters in Eq. (5) are able to completely reproduce the well depths of five characteristic configurations (Fig. 3). Taking

$$\nu_0 > 0, \tag{8}$$

Eqs. (6) and (7), together with the inequality $wd_a > wd_c$, imply

$$\nu_1 + 1 > 1 - \nu_1 > 0, \quad \text{i.e.} \quad 1 > \nu_1 > 0. \tag{9}$$

Proceeding similarly with inequalities between well depths of the other configurations in Fig. 3, we find

$$\nu_1 + \nu_2 > \nu_3, \tag{10}$$

$$\nu_1 < \nu_3 - 1. \tag{11}$$

The condition $wd_a > wd_b > wd_c$ gives upper and lower bounds on ε_e as

$$\left(\frac{1+\nu_1}{1-\nu_1+2\nu_2+\nu_3}\right)^{\nu_0} > \varepsilon_e > \left(\frac{1-\nu_1}{1-\nu_1+2\nu_2+\nu_3}\right)^{\nu_0}. \tag{12}$$

The inequalities (8)–(12) serve in checking the consistency of any simple choice of the parameters.

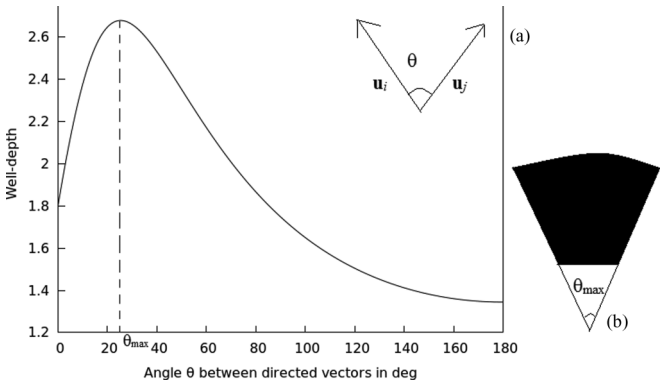

FIG. 5. Curvature: (a) Well depth $\varepsilon_{\rm wd}$ [Eq. (5)] as a function of interim angle θ between two directed ellipsoids with directed axes $\hat{\mathbf{u}}_i$ and $\hat{\mathbf{u}}_j$ making equal angles with the line joining their centers (inset). Choice of parameters: $\nu_0 = 1$, $\nu_1 = 0.8$, $\nu_2 = 4$, $\nu_3 = 3$, $\varepsilon_e = 0.12$, and $\varepsilon_0 = 1$. (b) Equivalent packing parameter model in black.

As we move from the most preferred configuration a in Fig. 3 to the next preferred one b by gradually increasing the angle θ between the spheroids [see inset of Fig. 5(a)], $\hat{\mathbf{u}}_i \cdot \hat{\mathbf{u}}_j$ and ε_{GB} decrease while $\hat{\mathbf{u}}_i \cdot \hat{\mathbf{r}} - \hat{\mathbf{u}}_j \cdot \hat{\mathbf{r}}$ and $-(\hat{\mathbf{u}}_i \cdot \hat{\mathbf{r}})(\hat{\mathbf{u}}_j \cdot \hat{\mathbf{r}})$ increase. This implies a crossover with a maximum $\varepsilon_{\rm wd}$ [Eq. (5)] at some θ, say $\theta_{\rm max}$, between 0 and π [Fig. 5(a)]. This orientation, with one spheroid inclined to another at angle $\theta_{\rm max}$, is arguably the most preferred (i.e., minimum energy) orientation between a pair of spheroids. The spheroids therefore, would prefer to pack in clusters like cones with angle $\theta_{\rm max}$ [Fig. 5(b)]. Hence, the effective packing parameter [34] of our model spheroids is dependent on $\theta_{\rm max}$. Other model parameters remaining constant, $\theta_{\rm max}$ increases with increasing ε_e. Therefore ε_e can be regarded as the parameter governing phase curvature or packing parameter. For example, the other parameters remaining constant, double-chain lipids forming flat bilayers will have smaller ε_e compared to single-chain surfactants forming globular micelles.

In view of the above discussion, our single-site model amphiphile can be interpreted as any amphiphile with a polar head and apolar tail(s) treating both the hydrated headgroup and the hydrophobic and lipophilic tail interactions implicitly. It may be noted that mixtures of amphiphiles of different species can easily be modeled by choosing parameters of the interspecies interaction differently from the intraspecies ones. However, all species must have the same length as interaction between spheroids of two different lengths has no interpretation in our model.

III. COMPUTER SIMULATIONS

In absence of any explicit aqueous phase for pressure coupling, *NVT* molecular dynamics (MD) was performed instead of *NPT* with the above model for systems of identical amphiphiles [35,36]. The Nosé-Hoover (NH) algorithm was employed for the canonical thermostating [37,38]. Translational and rotational degrees of freedom were thermostated separately [39]. Sufficiently large time steps were used without compromising the desired conservation of an appropriate quantity that remains conserved in NH MD [39]. A simple integrator for linear molecules was used to rotate the uniaxial spheroids [40]. Periodic boundary conditions and a fixed cubic simulation box were employed for all the simulations. System sizes (number of amphiphiles in the simulation box) chosen

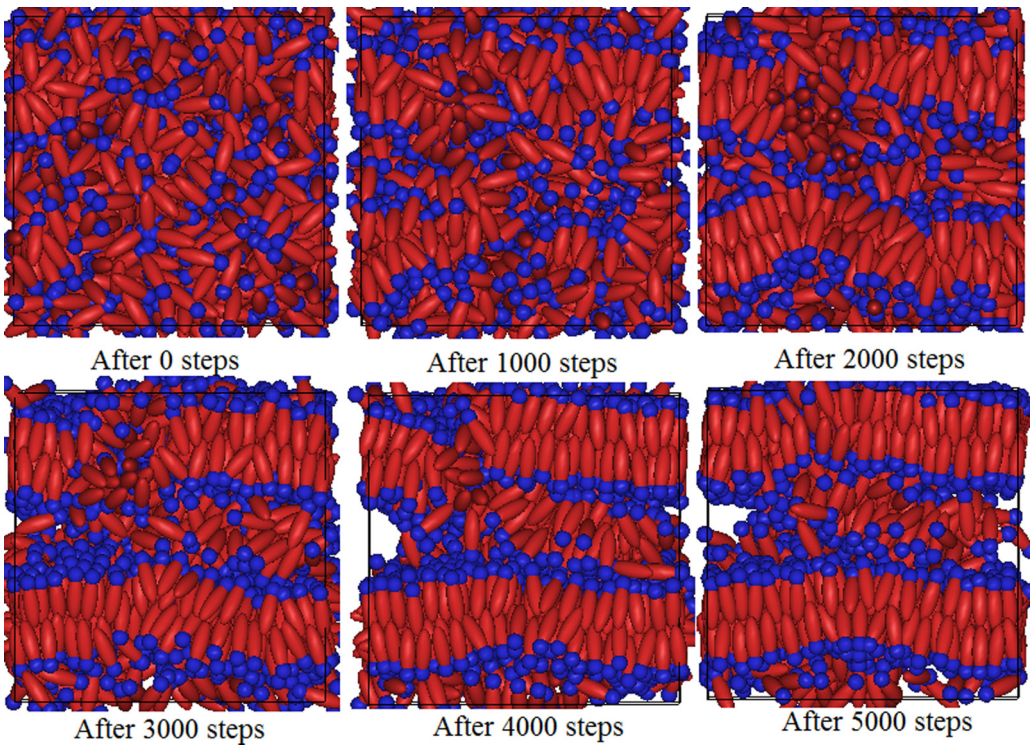

FIG. 6. Dark spheres signify headgroups for directed surfactants. Self-assembly into bilayers from randomized initial configuration for parameters as in Fig. 7(a). Integration time step: 0.0025.

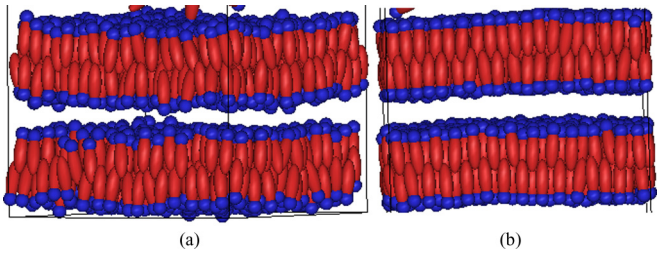

FIG. 7. Stable bilayers from 1372 particles (number density = 0.17) for $\nu_0 = 1$, $\nu_1 = 0.8$, $\nu_2 = 4$, $\nu_3 = 3$, $\varepsilon_e = 0.052$, $\sigma_e = 3$, $range = 3$, and amphiphile moment of inertia = 4. (a) Fluid phase (temperature = 2.5); (b) gel phase (temperature = 1).

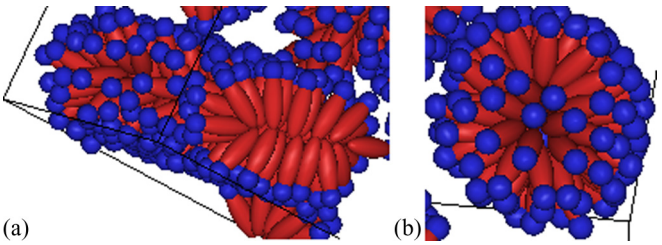

FIG. 9. Curved phases from 500 particles (number density = 0.1) for $\nu_0 = 1$, $\nu_1 = 0.8$, $\nu_2 = 4$, $\nu_3 = 3$, $\sigma_e = 3$, $range = 3$, amphiphile moment of inertia = 4, and temperature = 2. (a) Box spanning cylinder ($\varepsilon_e = 0.11$); (b) micelle ($\varepsilon_e = 0.15$).

were 256, 500, 1372, and 6912. Reduced units (meaning $\sigma_0 = 1$, $\varepsilon_0 = 1$ and amphiphile mass = 1) were used throughout.

Self-assembly from randomized initial configurations was found to be quite rapid with aggregates forming within 3000 (spherical micelles) to 4000 (bilayers) steps. Figure 6 shows a series of snapshots at 1000 step intervals starting from the randomized gas phase. Within 4000 steps the bilayers become quite recognizable. Increasing ε_e [within the bounds defined in Eq. (12)] while retaining the rest of the parameters, phases with more and more positive curvature were obtained. This trend was consistently reproduced for varied choices of parameters and system sizes. For a given choice of parameters and system size, phases at different number densities were studied, though no systematic exploration of the phase diagram was attempted.

Aggregate stability was checked by complete disassembly through heating followed by cooling to the temperature under study. The phases, if regained, would most likely be stable. Under suitable conditions (density or box dimension) box-spanning stable bilayers forming a multibilayer neat phase [6] were obtained. Figure 7(a) depicts such a neat phase with two bilayers in the cubic simulation box at temperature 2.5 for 1372 amphiphiles (of length $\sigma_e = 3$ and moment of inertia = 4) with number density 0.17. The model parameters used were $\nu_0 = 1$, $\nu_1 = 0.8$, $\nu_2 = 4$, $\nu_3 = 3$, $\varepsilon_e = 0.052$, and $range = 3$. The integration time step was 0.0025. Note that the effective treatment of hydration pressure keeps the two bilayers apart. In other cases, many bilayer patches or disc-shaped micelles remained in the simulation box. Sometimes multiply connected ramp structures were observed. Although no sealed vesicles were obtained, curved bilayers reminiscent of vesicular cross sections were observed at large system sizes (of the order of 1000 particles in the simulation box). Configurations such as pores, passages, and necks were also observed at these system sizes [41]. At lower temperatures (comparable to or lower than 1) crystal-like gel phases [Fig. 7(b)] were observed for low values of ε_e as opposed to the fluid bilayer phases for higher temperatures (greater than 1). Fluidity was apparent when the time series of root-mean-square displacement showed an increasing trend [35] [Fig. 8(a)]. Another characteristic feature of the fluidity is the loss of hexagonal order in the bilayer plane [Fig. 8(b)]. With increasing length of the model spheroid (from $\sigma_e = 3$ to $\sigma_e = 5$) the (gel-like) smectic-*A* [6] configuration gained more thermal stability and interdigitation became prominent.

For high ε_e, spherical micelles were obtained. An example is provided in Fig. 9(b) for parameters given in the caption. However, micellization was always observed above some threshold density, thus mimicking the critical micelle concentration. Thanks to our hydration force modeling by repulsive interactions, unphysical clustering of micelles [16] was never observed. Micelles were also found to arrange themselves in a cubic crystal as in an isotropic phase [6]. For ε_e with values interim between the bilayers and spherical micelles, cylindrical

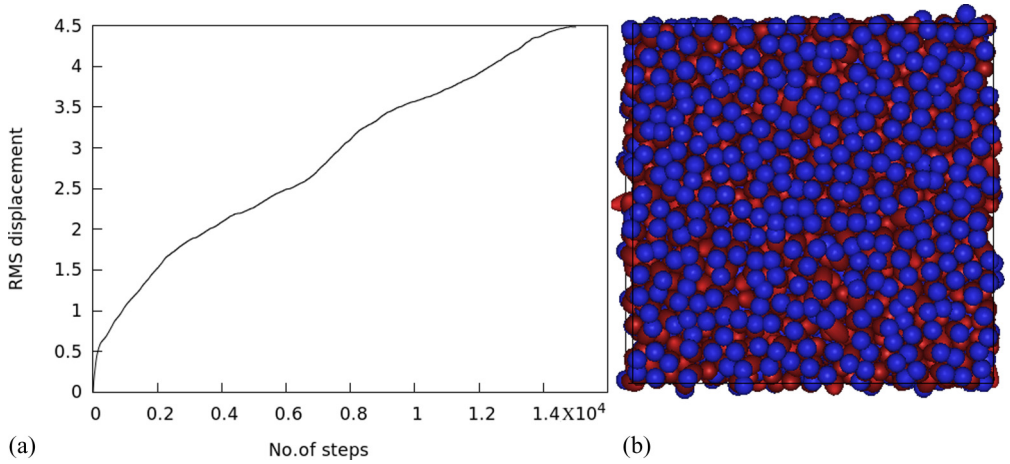

FIG. 8. Bilayer fluidity: (a) Postequilibration root-mean-square (rms) displacement for 15 000 steps starting from the configuration in Fig. 7(a). Integration time step size = 0.0025 in reduced units. (b) No hexagonal order in bilayer plane for bottom leaflet in Fig. 7(a).

and ellipsoidal micelles were found often in coexistence with spherical micelles. Box-spanning cylinders sometimes were also generated [Fig. 9(a)]. Micelles were generally seen to be thermally more stable compared to bilayers.

IV. DISCUSSIONS: SCOPE

To conclude, a packing parameter based, single-site model amphiphile has been presented that treats water-mediated interactions implicitly with simple pair potential. The model successfully shows rapid unassisted self-assembly into phases with diverse morphology. It is a direct representation of a tunable packing parameter without compromising self-assembly. Being nonspecific, simple, and solvent-free, it is suitable for qualitative mesoscopic studies aimed towards a fundamental understanding of collective molecular behavior such as amphiphile mixing, domain formation, and elasticity in aggregates ranging from cellular lipid bilayers to synthetic copolymer micelles. With lower computational demand thanks to the effective molecular-level coarse graining, such a model may also encourage suggestive pilot simulations of technological and medical importance with follow up by higher resolution modeling later on. As a specific example, dynamical studies of self-assembly of liposomal drug carriers and their fusion with cellular biomolecular aggregates such as lipid bilayer vesicles (endosomes) and membranes may be taken up with the present model and its possible future extensions.

This paper responds to a long-standing need for an efficient single-site model in the context of simulating large scale phenomena emerging from aggregation of nanoscale molecules in solution. Studies of these lyotropic phases are scarce compared to thermotropic liquid crystals due to severe computational demand in simulating amphiphile solutions. Simple, single-site, anisotropic interaction models such as Gay-Berne ellipsoids have contributed significantly to thermotropic studies. With the present model the same is hoped in connection to the more versatile field of lyotropic liquid crystals.

ACKNOWLEDGMENTS

One of the authors (S.D.) is grateful to Council of Scientific & Industrial Research (CSIR), India for financial assistance in terms of a Junior Research Fellowship under File No. 09/028(0960)/2015-EMR-I. Simulations were run on computers provided under the UPE-UGC scheme.

APPENDIX: EXPRESSIONS FOR FORCES AND TORQUES

The force exerted on amphiphile i by amphiphile j is $\mathbf{F}_{ij} = -\overrightarrow{\nabla}_{\mathbf{r}} V$ and that on j by i is $\mathbf{F}_{ji} = -\mathbf{F}_{ij}$. Now,

$$\begin{aligned}\overrightarrow{\nabla}_{\mathbf{r}} V &= \frac{\partial V}{\partial r}\hat{\mathbf{r}} + \frac{1}{r}[\overrightarrow{\nabla}_{\hat{\mathbf{r}}} V - \{(\overrightarrow{\nabla}_{\hat{\mathbf{r}}} V)\cdot\hat{\mathbf{r}}\}\hat{\mathbf{r}}] \\ &= \left\{\frac{\partial V}{\partial r} - \frac{(\overrightarrow{\nabla}_{\hat{\mathbf{r}}} V)\cdot\hat{\mathbf{r}}}{r}\right\}\hat{\mathbf{r}} + \frac{1}{r}\overrightarrow{\nabla}_{\hat{\mathbf{r}}} V. \end{aligned} \tag{A1}$$

The torque on i due to j is given by $\mathbf{T}_{ij} = -\hat{\mathbf{u}}_i \times \overrightarrow{\nabla}_{\hat{\mathbf{u}}_i} V$ and that due to i on j, by $\mathbf{T}_{ji} = -\hat{\mathbf{u}}_j \times \overrightarrow{\nabla}_{\hat{\mathbf{u}}_j} V$. However, $\mathbf{F}_{ij}$, $\mathbf{T}_{ij}$, and $\mathbf{T}_{ji}$ are related by the vector equation, $\mathbf{T}_{ji} + \mathbf{T}_{ij} + \mathbf{r}\times\mathbf{F}_{ij} = 0$. This follows directly from the rotational invariance of $V(r,\hat{\mathbf{r}},\hat{\mathbf{u}}_i,\hat{\mathbf{u}}_j)$ [42]. It is, therefore, sufficient to have the expressions for $\partial V/\partial r$, $\overrightarrow{\nabla}_{\hat{\mathbf{r}}} V$, and $\overrightarrow{\nabla}_{\hat{\mathbf{u}}_i} V$ in order to obtain all the necessary forces and torques from them. Now,

$$\begin{aligned}\frac{\partial V}{\partial r} &= -24\varepsilon_0(2R^{-13} - R^{-7})/\sigma_0, \ \text{if } r < r_l \\ &= \frac{6(r_u - r)(r - r_l)\varepsilon_{\mathrm{wd}}(\hat{\mathbf{r}},\hat{\mathbf{u}}_i,\hat{\mathbf{u}}_j)}{range^3}, \ \text{if } r_l \leqslant r < r_u \\ &= 0, \ \text{otherwise.}\end{aligned} \tag{A2}$$

Additionally,

$$\begin{aligned}\overrightarrow{\nabla}_{\hat{\mathbf{r}}/\hat{\mathbf{u}}_i} V &= -\frac{\partial V}{\partial r}\overrightarrow{\nabla}_{\hat{\mathbf{r}}/\hat{\mathbf{u}}_i}\sigma_{\mathrm{GB}} - \overrightarrow{\nabla}_{\hat{\mathbf{r}}/\hat{\mathbf{u}}_i}\varepsilon_{\mathrm{wd}}, \ \text{if } r < r_l \\ &= s(r)\overrightarrow{\nabla}_{\hat{\mathbf{r}}/\hat{\mathbf{u}}_i}\varepsilon_{\mathrm{wd}}, \ \text{if } r_l \leqslant r < r_u \\ &= 0, \ \text{otherwise.}\end{aligned} \tag{A3}$$

Writing $[\nu_1(\hat{\mathbf{u}}_i\cdot\hat{\mathbf{u}}_j) + \nu_2(\hat{\mathbf{u}}_i\cdot\hat{\mathbf{r}} - \hat{\mathbf{u}}_j\cdot\hat{\mathbf{r}}) - \nu_3(\hat{\mathbf{u}}_i\cdot\hat{\mathbf{r}})(\hat{\mathbf{u}}_j\cdot\hat{\mathbf{r}}) + 1]$ as ε', Eq. (5) becomes

$$\varepsilon_{\mathrm{wd}} = \varepsilon_0\varepsilon'^{\nu_0}\varepsilon_{\mathrm{GB}}. \tag{A4}$$

Hence,

$$\overrightarrow{\nabla}_{\hat{\mathbf{r}}/\hat{\mathbf{u}}_i}\varepsilon_{\mathrm{wd}} = \nu_0\frac{\varepsilon_{\mathrm{wd}}}{\varepsilon'}\overrightarrow{\nabla}_{\hat{\mathbf{r}}/\hat{\mathbf{u}}_i}\varepsilon' + \varepsilon_0\varepsilon'^{\nu_0}\overrightarrow{\nabla}_{\hat{\mathbf{r}}/\hat{\mathbf{u}}_i}\varepsilon_{\mathrm{GB}}. \tag{A5}$$

Now,

$$\overrightarrow{\nabla}_{\hat{\mathbf{r}}}\varepsilon' = \nu_2(\hat{\mathbf{u}}_i - \hat{\mathbf{u}}_j) - \nu_3[(\hat{\mathbf{u}}_j\cdot\hat{\mathbf{r}})\hat{\mathbf{u}}_i + (\hat{\mathbf{u}}_i\cdot\hat{\mathbf{r}})\hat{\mathbf{u}}_j], \tag{A6}$$

and

$$\overrightarrow{\nabla}_{\hat{\mathbf{u}}_i}\varepsilon' = \nu_1\hat{\mathbf{u}}_j + [\nu_2 - \nu_3(\hat{\mathbf{u}}_j\cdot\hat{\mathbf{r}})]\hat{\mathbf{r}}. \tag{A7}$$

The last pieces needed, therefore, are $\overrightarrow{\nabla}_{\hat{\mathbf{r}}/\hat{\mathbf{u}}_i}\sigma_{\mathrm{GB}}$ and $\overrightarrow{\nabla}_{\hat{\mathbf{r}}/\hat{\mathbf{u}}_i}\varepsilon_{\mathrm{GB}}$. Note that by defining

$$\begin{aligned}g(x) &= \frac{1}{2}\left\{\frac{(\hat{\mathbf{r}}\cdot\hat{\mathbf{u}}_i + \hat{\mathbf{r}}\cdot\hat{\mathbf{u}}_j)^2}{1 + x(\hat{\mathbf{u}}_i\cdot\hat{\mathbf{u}}_j)} + \frac{(\hat{\mathbf{r}}\cdot\hat{\mathbf{u}}_i - \hat{\mathbf{r}}\cdot\hat{\mathbf{u}}_j)^2}{1 - x(\hat{\mathbf{u}}_i\cdot\hat{\mathbf{u}}_j)}\right\} \\ &= \frac{(\hat{\mathbf{r}}\cdot\hat{\mathbf{u}}_i)^2 + (\hat{\mathbf{r}}\cdot\hat{\mathbf{u}}_j)^2 - 2x(\hat{\mathbf{r}}\cdot\hat{\mathbf{u}}_i)(\hat{\mathbf{r}}\cdot\hat{\mathbf{u}}_j)(\hat{\mathbf{u}}_i\cdot\hat{\mathbf{u}}_j)}{1 - x^2(\hat{\mathbf{u}}_i\cdot\hat{\mathbf{u}}_j)^2},\end{aligned} \tag{A8}$$

we have $\sigma_{\mathrm{GB}} = \sigma_0/\sqrt{1 - \chi g(\chi)}$ and $\varepsilon_{\mathrm{GB}} = 1 - \chi' g(\chi')$. Hence, the knowledge of $\overrightarrow{\nabla}_{\hat{\mathbf{r}}/\hat{\mathbf{u}}_i} g(x)$ gives $\overrightarrow{\nabla}_{\hat{\mathbf{r}}/\hat{\mathbf{u}}_i}\sigma_{\mathrm{GB}}$ and $\overrightarrow{\nabla}_{\hat{\mathbf{r}}/\hat{\mathbf{u}}_i}\varepsilon_{\mathrm{GB}}$. Now,

$$\overrightarrow{\nabla}_{\hat{\mathbf{r}}} g(x) = 2\frac{\zeta_j^i\hat{\mathbf{u}}_i + \zeta_i^j\hat{\mathbf{u}}_j}{1 - x^2(\hat{\mathbf{u}}_i.\hat{\mathbf{u}}_j)^2}, \tag{A9}$$

where $\zeta_j^i = \hat{\mathbf{r}}\cdot\hat{\mathbf{u}}_i - x(\hat{\mathbf{r}}\cdot\hat{\mathbf{u}}_j)(\hat{\mathbf{u}}_i\cdot\hat{\mathbf{u}}_j)$, and

$$\overrightarrow{\nabla}_{\hat{\mathbf{u}}_i} g(x) = 2\frac{\zeta_j^i\hat{\mathbf{r}} + x[x(\hat{\mathbf{u}}_i\cdot\hat{\mathbf{u}}_j)g(x) - (\hat{\mathbf{r}}\cdot\hat{\mathbf{u}}_i)(\hat{\mathbf{r}}\cdot\hat{\mathbf{u}}_j)]\hat{\mathbf{u}}_j}{1 - x^2(\hat{\mathbf{u}}_i\cdot\hat{\mathbf{u}}_j)^2}. \tag{A10}$$

[1] D. Evans and H. Wennerström, *The Colloidal Domain: Where Physics, Chemistry, Biology and Technology Meet* (VCH Verlagsgesellschaft, Weinheim, 1994).

[2] W. Hoffmann, in *The Formation of Micelles. Thermodynamic Data for Biochemistry and Biotechnology*, edited by H. J. Hinz (Springer-Verlag, Berlin, 1986).

[3] R. J. Hunter, *Foundations of Colloid Science* (Clarendon Press, Oxford, 1987).

[4] J. N. Israelachvili, *Intermolecular and Surface Forces* (Academic Press, London, 1991).

[5] K. Shinoda, *Principle of Solution and Solubility* (Marcel Dekker, New York, 1978).

[6] E. B. Priestley, P. J. Wojtowicz, and P. Sheng, *Introduction to Liquid Crystals* (Plenum Press, New York and London, 1974).

[7] C. Tanford, J. Phys. Chem. **76**, 3020 (1972).

[8] W. Helfrich, J. Phys.: Condens. Matter **6**, A79 (1994).

[9] S. M. Gruner, J. Phys. Chem. **93**, 7562 (1989).

[10] D. T. Allen and C. D. Lorenz, J. Self-Assem. Mol. Electron. **3**, 1 (2015).

[11] S. J. Marrink, A. H. de Vries, and A. E. Mark, J. Phys. Chem. B **108**, 750 (2004).

[12] M. Orsi and J. W. Essex, PLoS One **6**, e28637 (2011).

[13] I. R. Cooke, K. Kremer, and M. Deserno, Phys. Rev. E **72**, 011506 (2005).

[14] G. Brannigan, P. F. Phillips, and F. L. H. Brown, Phys. Rev. E **72**, 011915 (2005).

[15] A. J. Sodt and T. Head-Gordon, J. Chem. Phys. **132**, 205103 (2010).

[16] C. Arnarez, J. J. Uusitalo, M. F. Masman, H. I. Ingólfsson, D. H. de Jong, M. N. Melo, X. Periole, A. H. de Vries, and S. J. Marrink, J. Chem. Theory Comput. **11**, 260 (2015).

[17] Absence of molecular flexibility in single-site models, as opposed to the bead-based ones, simplifies and speeds up the algorithm without much loss and stiff models have indeed been applied profitably in amphiphile simulations [Farago *et al.*, Phys. Rev. Lett. **96**, 018102 (2006); Sun and Gezelter, J. Phys. Chem. B **112**, 1968 (2008); Farago and Pincus, J. Chem. Phys. **120**, 2934 (2004)].

[18] J. G. Gay and B. J. Berne, J. Chem. Phys. **74**, 3316 (1981).

[19] G. R. Luckhurst, Liq. Cryst. **33**, 1389 (2006).

[20] For example, the GB fluid (molecular-level single-site model) has a phase diagram with a well-characterized nematic-isotropic transition temperature, while apparently its Lennard-Jones counterpart (multibead, multisite model) does not show any phase transition of this kind when only the temperature is varied [Penna *et al.*, Eur. Phys. J. E **5**, 259 (2001)].

[21] I. R. Cooke and M. Deserno, J. Chem. Phys. **123**, 224710 (2005).

[22] G. Brannigan and F. L. H. Brown, J. Chem. Phys. **120**, 1059 (2004).

[23] H. Noguchi, J. Chem. Phys **134**, 055101 (2011).

[24] J. N. Israelachvili, D. J. Mitchell, and B. W. Ninham, J. Chem. Soc., Faraday Trans. 2 **72**, 1525 (1976).

[25] W. Kunz, F. Testard, and T. Zemb, Langmuir **25**, 112 (2009).

[26] R. P. Rand and V. A. Parsegian, Biochim. Biophys. Acta **988**, 351 (1989).

[27] Equation (3) is formally similar to $V_{\rm rep} + V_{\rm attr}$ in Ref. [13]. Here, however, we replace the original $\cos^2$ function [13] by a computationally simpler $s(r)$ since sufficient broadness of the attractive tail is all that matters [21].

[28] G. Brannigan and F. L. H. Brown, in *Coarse-Graining of Condensed Phase and Biomolecular Systems*, edited by G. A. Voth (CRC Press, Taylor & Francis Group, Boca Raton, London, New York, 2009).

[29] C. Tanford, Science **200**, 1012 (1978).

[30] N. T. Southall, K. A. Dill, and A. D. J. Haymet, J. Phys. Chem. B **106**, 521 (2002).

[31] C. Tanford, *The Hydrophobic Effect: Formation of Micelles and Biological Membranes* (Wiley, New York, 1980).

[32] D. Chandler, Nature **437**, 640 (2005).

[33] C. Tanford, Proc. Natl. Acad. Sci. USA **76**, 4175 (1979).

[34] The packing parameter incorporates a thermodynamic-geometric model whereby an amphiphile in stable aggregates is represented as an oblong molecule shaped just so that such molecules can closely fit together into an aggregate of the correct curvature. Actually, the packing parameter is defined as the ratio between a steric tail area (lateral cross section) and an equilibrium headgroup area of the amphiphile in aggregate [24,25]. Hence, for constant molecular length, decreasing packing parameter means increasing curvature.

[35] M. P. Allen and D. J. Tildesley, *Computer Simulation of Liquids* (Clarendon Press, Oxford, 1987).

[36] D. Frenkel and B. Smit, *Understanding Molecular Simulation* (Academic Press, New York, 1996).

[37] W. G. Hoover, Phys. Rev. A **31**, 1695 (1985).

[38] B. L. Holian, A. F. Voter, and R. Ravelo, Phys. Rev. E **52**, 2338 (1995).

[39] S. Nosé, Mol. Phys. **57**, 187 (1986).

[40] A. Dullweber, B. Leimkuhler, and R. McLachlan, J. Chem. Phys. **107**, 5840 (1997).

[41] D. Constantin and P. Oswald, Phys. Rev. Lett. **85**, 4297 (2000).

[42] M. P. Allen and G. Germano, Mol. Phys. **104**, 3225 (2006).